

# Synthesis and Catalytic Activity of Spinel Ferrites: A Brief Review

Sagar Kumar Dutta <sup>1,\*</sup>, Morsheda Akhter <sup>1</sup>, Jamil Ahmed <sup>1,\*</sup>, Md. Khairul Amin <sup>1</sup>, Palash Kumar Dhar <sup>1</sup>

<sup>1</sup> Chemistry Discipline, Khulna University, Khulna-9208, Bangladesh; sagar@ku.ac.bd (S.K.D.); morshdaakhter.51@gmail.com (M.A.); jamil@ku.ac.bd (J.A.); khairul.che@ku.ac.bd (K.A.); palash10ku@gmail.com (P.K.D.);

\* Correspondence: jamil@ku.ac.bd (J.A.); sagar@ku.ac.bd (S.K.D.);

Received: 8.06.2021; Revised: 20.07.2021; Accepted: 24.07.2021; Published: 15.08.2021

**Abstract:** The spinel ferrites have earned enormous interest worldwide because of their attractive potential applications. This review highlights different synthetic protocols of spinel ferrites such as coprecipitation, sol-gel, microemulsion, solid-state, hydrothermal, and thermal decomposition, where each method can influence the properties of ferrites. The use of ferrites in heterogeneous catalysis of various organic syntheses is discussed therein; the activity is mostly particle size-dependent. The catalytic activity of spinel ferrites towards photo-irradiated dye degradation is also studied. In the presence of H<sub>2</sub>O<sub>2</sub> producing a Fenton-type system, ferrites have tremendous potential for dye degradation in an advanced oxidation process.

**Keywords:** synthesis; ferrite; photocatalytic activities; dye degradation; heterogeneous catalyst.

© 2021 by the authors. This article is an open-access article distributed under the terms and conditions of the Creative Commons Attribution (CC BY) license (<https://creativecommons.org/licenses/by/4.0/>).

## 1. Introduction

Spinel ferrites' considerable interest to the researchers exhibits their versatile applications in fabricating various electrical devices, chemical sensors, catalysis wastewater treatment, magnetic separation, transducers, transformers, actuators, etc. [1,2]. Ferrites are composed of iron oxide, blended with a small amount of some other metal oxides [3-5]. On the other hand, spinel structures have the general formula of AB<sub>2</sub>O<sub>4</sub>, where the metallic cations A and B occupy two different crystallographic sites, tetrahedral (A site) and octahedral (B site); which are coordinated to the oxygen atoms [6,7]. In this formula AB<sub>2</sub>O<sub>4</sub>, when there is a Fe<sup>3+</sup> ion present, the structure would be termed as ferrite. Therefore, the general formula of spinel ferrite would be MFe<sub>2</sub>O<sub>4</sub> (where M = Divalent metal cations) [8-10]. They have a face-centered cubic structure. Along with spinel structure, ferrites can exist in different crystallographic states such as garnet (M<sub>3</sub>Fe<sub>5</sub>O<sub>12</sub>; M = rare earth cations), hexaferrite (SrFe<sub>12</sub>O<sub>19</sub> and BaFe<sub>12</sub>O<sub>19</sub>), and orthoferrite (MFeO<sub>3</sub>; M = rare earth cations) [3, 11]. Amongst them, spinel ferrites have got special attention because of their interesting properties and applications [11].

Generally, in spinel ferrites, the tetrahedral sites (A-sites) are occupied by the divalent cations like Mg<sup>2+</sup>, Fe<sup>2+</sup>, Co<sup>2+</sup>, Cd<sup>2+</sup>, Cu<sup>2+</sup>, Zn<sup>2+</sup>, etc., while the octahedral sites (B-sites) are occupied by trivalent cations like Fe<sup>3+</sup>, Al<sup>3+</sup>, Gd<sup>3+</sup>, Dy<sup>3+</sup>, Eu<sup>3+</sup>, and Tb<sup>3+</sup>, etc. [12,13]. Depending on the distribution of cations in the structure, there can be three types of spinel structures based on the cation distribution on these two sites: (a) Normal spinel where M<sup>2+</sup> occupies A-sites and trivalent cations on B-sites; (b) Inverse spinel where divalent cations (M<sup>2+</sup>) occupy the B-sites and trivalent cations occupy half of the A-sites and half of the B-sites

by equal distribution (c) Mixed spinel in which both divalent and trivalent cations occupy A and B-sites [14-16]. The physical and chemical properties of spinel ferrites depend on the type and distribution of cations on different sites as well as on the morphological properties [6, 17]. The morphology of different spinel ferrites can be controlled by altering the elemental composition and criterion of synthesis like sintering temperature, sintering time, rate of heating and cooling, etc. [18-21]. Hence a suitable synthetic approach is essential to attain the desired functions.

Nowadays, ferrites are being used as a potential material for heterogeneous catalysis in organic synthesis [22,23], becoming an alternative to the catalysts typically used. On the other hand, the activity of spinel ferrites as photocatalysts for the degradation of organic pollutants, especially for dye, is very familiar [22]. The use of hydrogen peroxide as an oxidant in the catalytic process develops a Fenton reaction system [23] and significantly increases the catalyst's effectiveness. The major advantages of spinel ferrite particles being used as a catalyst are their magnetic properties and the ease of retrievability and recyclability of the catalysts after completion of the reaction. The present review aims to analyze the usability of different synthetic methods of spinel ferrites.

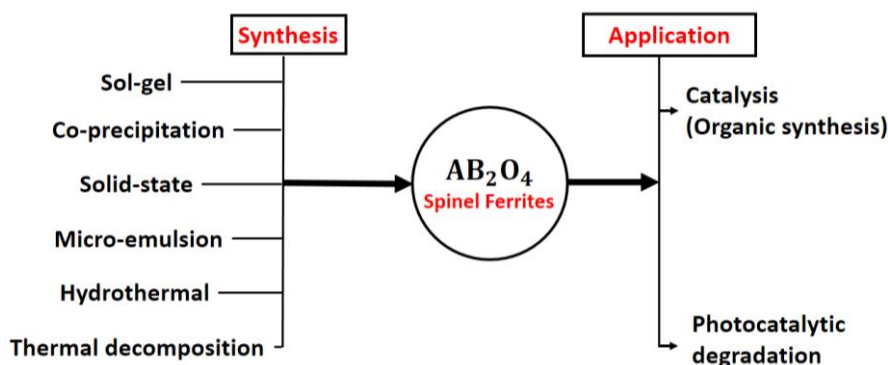


**Figure 1.** Overview of recent work.

## 2. Synthesis of Spinel Ferrites

Although there are many synthetic approaches to preparing spinel ferrite nanoparticles, including chemical co-precipitation, thermal decomposition, hydrothermal, sol-gel, solid-state reaction, microemulsion, etc., most of them have major drawbacks over their advantages.

### 2.1. Chemical co-precipitation.

Co-precipitation is a simple, easily accessible, and most frequently used method for synthesizing ferrite particles. The major advantages of this method are the size and homogeneity of the particles can be controlled by controlling reaction temperature, stirring speed, pH, the concentration of the solution, rate of addition of alkali, etc. [24-26]. Thus, particles of smaller sizes with enhanced reactivity can be obtained [27,28].

In a typical procedure, metal salts with a stoichiometric ratio are dissolved in water. As nanoparticles tend to agglomerate, therefore, a surfactant mostly oleic acid, sodium dodecyl sulfate, polyacrylic acid, etc., is added to the mixture to avoid agglomeration. Reaction to form hydroxide from metal salts occurs when the pH of the solution is increased, generally between 10-13, by adding alkali solution to get a high yield. The mixture is then heated at 60-100 °C temperature with constant stirring for a long time for the complete conversion into ferrite

particles. Then the mixture is cooled down, the particles are separated and washed several times by water and/or ethanol/acetone to remove the impurities, and then dried in an oven at 50-100 °C overnight. Finally, the dried product is calcined in a furnace at a higher temperature ( $\geq 400^{\circ}\text{C}$ ) in various time durations to observe the effect of calcination [29-37]. In order to get a better crystallinity, a higher calcining temperature is needed [20], which would be a limitation of this method. Also, the pH needs to be set to near neutral during the washing; otherwise, particles could be agglomerated [38].

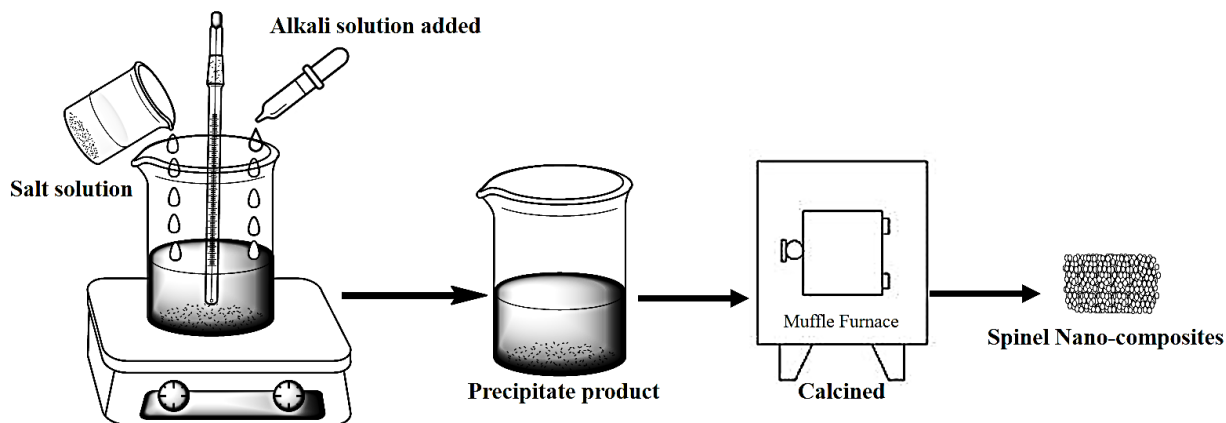


**Figure 2.** Chemical co-precipitation synthesis method of spinel nanocomposite.

## 2.2. Sol-gel method.

The method Sol-gel is known for its simplicity, controlled morphology, small particle size, and low reaction time. Originally, the method involves metal alkoxide as the precursor, which can be modified with metal salts, which undergo hydrolysis and condensation, and a gel formation occurs. A fuel (an organic complexant) is used to cause the condensation polymerization to take place. In a general procedure, metal alkoxides or metal salts are dissolved in a minimum amount of water, mixed together, and heated at 60-150 °C; thus, sol formation by hydrolysis occurs. The fuel (such as citric acid, urea, glycine, starch, etc.) is added to the mixture, which plays a vital role in the morphology and phase formation. The fuel makes the gel formation happen via polycondensation followed by syneresis or aging, where condensation continues within the gel networks and often expulsion of solvent due to shrinking. The gel is further dried, and a dense *xerogel* is formed. Finally, it is calcined at a higher temperature to remove the metal-hydroxyl bond, and the final particle is obtained. A base such as ammonia solution is added to increase the pH (mostly at 7) to enhance metal cation binding to citrate ions. In this reaction, the metal salts act as oxidizers and complexant as reductants, and an exothermic, self-sustaining thermally-induced anionic redox reaction occurs in the *xerogel* [39-54].

Now, some reports have described the sol-gel process of ferrite synthesis having some modification with the materials, and thus mechanism described earlier, i.e., using ethylene glycol with citric acid. Originally this method is known as the '*Pechini process*' invented by Maggio Pechini in 1967, where a *polyesterification* occurs between citric acid and ethylene glycol, forming a viscous liquid of extended covalent network. Upon drying and heating this on a furnace, all organic substances are removed, and finally, the metal oxide is obtained. Polyvinyl alcohol can also be used, which will form a three-dimensional network. Also, citric acid has been replaced with ethylenediaminetetraacetic acid (EDTA), which has an advantage

with four carboxylate groups. But in this way, the ability to control the size and morphology is reduced as the metal cations are trapped in the polymer network [46, 55-61].

### 2.3. Micro-emulsion method.

The Micro-emulsion method is based on the dispersion of two relatively immiscible liquids stabilized by surfactant molecules. Both the normal micellar (oil-in-water) and reverse micellar (water-in-oil) procedures are employed to synthesize particles. This method got special attention because of its excellent particle size, shape, uniformity, and dispersity control. Particles with extremely small sizes can be obtained by this method [62-65].

Here, an emulsion mixture is obtained by mixing metal salts with a surfactant, a polar solvent (water), and a non-polar solvent in definite stoichiometry. Trimethylammonium bromide (CTAB) and sodium bis(2-ethylhexyl) sulfosuccinate (AOT) is the most extensively used surfactant. Poly (oxyethylene)-4-laurylether or *n*-butanol is used as a co-surfactant, and *n*-hexane, octanol, isooctane is used as the non-polar liquid. Solutions are mixed together afterward, a reducing agent is added and stirred with heat treatment (20-80°C). Thus, the particles are precipitated, separated, washed with water and ethanol, and finally dried in an oven. The reducing agent such as hydrazine, sodium borohydride, sodium hydroxide or ammonia solution makes the particle formed by increasing pH (9-12). Though the reaction takes place at a lower temperature is advantageous, but the synthesized particles are low crystalline in nature, also a large number of solvents is required [22, 66-72].

### 2.4. Solid-state reaction.

The solid-state method can be considered the simplest method of ferrite particle synthesis, where only heat treatment involves particle formation. This method is commercially advantageous because of its scope of less impure existence, also large-scale production.

In this method, metal oxide precursors in calculated stoichiometry are finely grounded and mixed for a long time to obtain a homogenous mixture. Then the mixture is pre-sintered in a furnace at a high temperature ( $\geq 700^\circ\text{C}$ ) as if the solid mixtures react together to form the particles. These pre-sintered particles are further ground into fine particles. Generally, the particles are pressed into pellets applying pressure and sintered to a much higher temperature. Though the method is simple and convenient, it also has some disadvantages, including higher sintering temperature for a long time. Precursors are also milled for a long time, thus not so time-efficient, and cannot be controlled if any unwanted phase formation occurs. Also, the control over particle size is less [73-77].

**Table 1.** A comparison of the available synthetic methods of preparing spinel ferrites under different conditions.

Synthesis methods	Example	Reaction Temperature (°C)	pH	Fuel/ surfactant/ solvent	Calcining temperature (°C)	Calcination period	Particle size (nm)	Ref.
Sol-gel	CoFe <sub>2</sub> O <sub>4</sub>	110	7	Ethylene glycol	550	4 h	77.21	[52]
				Glycerin			86.12	
				Urea			65.84	
	Fe <sub>3</sub> O <sub>4</sub>	40-120	-	Ethylene glycol	200	-	18	[78]
					400		25	
	CoMn <sub>0.2</sub> Fe <sub>1.8</sub> O <sub>4</sub>	60-90	-	Citric acid-ethylene glycol	400	2 h	~20	[56]
Co-precipitation	NiFe <sub>2</sub> O <sub>4</sub>	80	12	Oleic acid	600	10 h	~8	[36]
	Fe <sub>3</sub> O <sub>4</sub> -CA <sup>a</sup>	60	10.5	-	-	-	17-30	[79]
	MnFe <sub>2</sub> O <sub>4</sub>	70	11	-	400	2 h	200-290	[35]
Solid-state	MgFe <sub>2</sub> O <sub>4</sub> <sup>b</sup>	-	-	-	-	-	12.31	[80]

Synthesis methods	Example	Reaction Temperature (°C)	pH	Fuel/ surfactant/ solvent	Calcining temperature (°C)	Calcination period	Particle size (nm)	Ref.
	Ni <sub>0.65-x</sub> Mg <sub>x</sub> Zn <sub>0.35</sub> Fe <sub>2</sub> O <sub>4</sub> (0.00 ≤ x ≤ 0.16)	-	-	-	1250	2 h <sup>c</sup>	480-1560	[81]
Micro-emulsion	MgFe <sub>2</sub> O <sub>4</sub>	-	-	Poly (oxyethylene) nonylphenylether/ heptane	600	2 h	20.9 ± 4.3	[82]
	Fe <sub>3</sub> O <sub>4</sub> /Chitosan	60	-	Acetic acid, Triton X-100/ n-hexanol, cyclohexane	-	-	50-92	[68]
	Ni <sub>0.58</sub> Zn <sub>0.58</sub> Fe <sub>2</sub> O <sub>4</sub>	500	-	Sodium dioctyl sulfosuccinate, isoootane	1200	4 h	8.4	[83]
Hydrothermal	NiFe <sub>2</sub> O <sub>4</sub>	150	10	-	-	-	53	[84]
				Glycerol	-	-	13	
				Sodium dodecyl sulfate	-	-	12	
	CoFe <sub>2</sub> O <sub>4</sub>	150-180	9	-	500	4 h	34	[85]
Thermal decomposition	MnFe <sub>2</sub> O <sub>4</sub>	270	-	Benzyl ether-oleyl amine, oleic acid, 1,2-hexadecandiol	-	-	~18.9	[86]
	CoFe <sub>2</sub> O <sub>4</sub>	200-290	-	Benzyl ether, oleic acid	-	-	~9.1	[87]

a = Citric acid; b = Dried at 90°C for 2 h; c = Pre-sintered at 900°C for 4 h;

### 2.5. Hydrothermal method.

The hydrothermal method is another feasible way to synthesize spinel ferrites where control in the composition is high. The method is easily accessible, and particles with greater morphological properties can be obtained [88]. Metal salts in required stoichiometry are dissolved in water and mixed together by magnetic stirring. Reports are also available where the method is assisted by stabilizing agents like sodium dodecyl sulfate, glycerol, plant extract, etc. The pH of the mixture is increased to 9-12 by means of a base solution that plays a vital role in particle formation. After subsequent magnetic stirring, the mixture is then transferred to a Teflon-coated stainless-steel autoclave at 150-200°C in various time durations to complete the reaction. The particles formed are then washed with water and ethanol to neutral pH, dried in an oven, and finally calcined in a furnace to obtain the fine particles [84, 85, 88-91].

### 2.6. Thermal decomposition.

Thermal decomposition is another convenient method of spinel ferrite synthesis where monodispersed particles with smaller sizes and better crystallinity are obtained. Also, this method can employ in large-scale production [92,93]. This method obtains ferrite particles by thermal decomposition of organometallic precursors using organic solvents with a high boiling point and a stabilizing agent [94].

The organometallic precursors are mixed with organic solvent and surfactant using a magnetic stirrer in an inert atmosphere. The mixture's temperature is then increased much higher (≤350 °C) for sufficient time duration to form the monodispersed spinel ferrites. The mixture is then cooled, separated the particles, washed several times with ethanol/acetone, and then dried overnight [86, 87, 93-96]. Though fine particle size can be obtained by this method, this largely depends on the control over the reaction temperature. The method is not so cost-

effective, requires high energy, also not so environmentally friendly when using toxic substances as solvent.

**Table 2.** Advantages and limitations of synthesis methods of spinel ferrites.

Synthesis methods	Advantages	Limitations
Co-precipitation	Easy and simple synthesis	Low crystallinity
	Particle size and homogeneity control	Long time
	Reactivity of the product	Required pH control
Sol-gel	Controlled morphology	Lack of purity
	Small particle size	
Microemulsion	Excellent control over size and shape	Large number of solvents required
	Low temperature	Poor crystallinity
Solid-state	Simpler procedure	Higher calcining temperature
	Possibility of low impurity existence	Milling for a long time
	Large-scale production	No control over unwanted phase formation
Hydrothermal	High control of composition	Required special equipment
	Enhanced morphological properties	High reaction temperature
Thermal decomposition	Monodispersed and smaller size	High temperature
	Better crystallinity	Toxic substances can be used as a solvent
	Large-scale production	Required organic solvents

### 3. Catalytic activities of spinel ferrites

#### 3.1. Heterogeneous catalysis of the organic synthesis reaction

It has been stated that ferrites are an efficient material for catalysis. It can be used as a heterogeneous catalyst in organic reactions [22]. Both simple ferrites and mixed-metal ferrite composites are used for this purpose. Ferrite particles are stable, less toxic, and easily separable from the reaction mixture due to their magnetic properties [97]. Therefore, interest in ferrite catalyzed synthesis reactions is enormously [22, 98, 99] increasing.

The catalytic activity of spinel ferrites is site-dependent, i.e., the octahedral sites are catalytically active while the tetrahedral sites are not. This is because reactant species can be fairly coordinated to octahedral sites having a larger size. Therefore, knowledge about the site preference of the selected metal cations is important to explore their catalytic behavior. Spherical calcium ferrite ( $\text{CaFe}_2\text{O}_4$ ) particles prepared by the citrate gel method with a mean size of 500-600 nm are successively used for the selective oxidation of styrene. Dilute hydrogen peroxide ( $\text{H}_2\text{O}_2$ , 30%) is used as an oxidizing agent. The oxidation reaction yields benzaldehyde as a major product and phenylacetaldehyde as the minor one [22].



**Figure 3.** Selective oxidation of styrene using  $\text{H}_2\text{O}_2$  as oxidant and  $\text{CaFe}_2\text{O}_4$  as a catalyst.

Among spinel ferrites, copper ferrite ( $\text{CuFe}_2\text{O}_4$ ) is one of the most efficient catalysts.  $\beta$ ,  $\gamma$ -unsaturated ketone was synthesized from acid chloride and allyl bromide/ cinnamyl chlorides in THF (tetrahydrofuran) using copper ferrite as the catalyst. The same citrate gel method is also used where the particle size is found to be 20 nm; therefore, no additives, ligands, or co-catalyst are required [98].

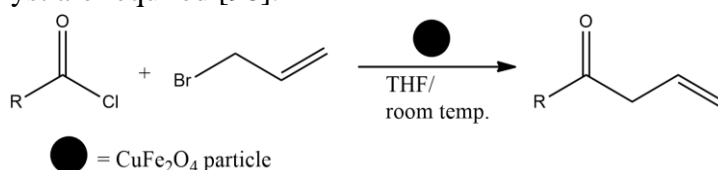


**Figure 4.**  $\beta$ ,  $\gamma$ -unsaturated ketone synthesis from allyl bromide in presence of spinel ferrite. R = (a)  $\text{C}_6\text{H}_5$  (b) 2- $\text{ClC}_6\text{H}_4$  (c) 2-Br, 5-F,  $\text{C}_6\text{H}_3$  (d) 2-Br, 5-F,  $\text{C}_6\text{H}_3$ , (e) Furanyl (f) 5-Phenyl, 3-Methyl, 4- Isoxazolyl, (g) 5-(2, 5-dichloro) Phenyl, 3-Methyl, 4Isoxazolyl, (h)  $(\text{CH}_3)_3\text{C}$ - (i)  $\text{C}_{11}\text{H}_{23}$ - (j)  $\text{C}_{15}\text{H}_{31}$ -

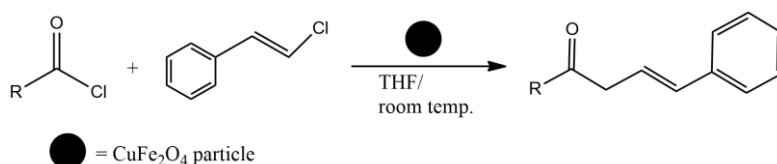


**Figure 5.**  $\beta$ ,  $\gamma$ -unsaturated ketone synthesis from cinnamyl chloride. R = (a) C<sub>6</sub>H<sub>5</sub> (b) 2-ClC<sub>6</sub>H<sub>4</sub> (c) Furanyl (d) -CH(CH<sub>3</sub>)<sub>2</sub>

25 nm-sized cobalt ferrite (CoFe<sub>2</sub>O<sub>4</sub>) synthesized by the co-precipitation method was used as a catalyst for oxidation of alkene to epoxide or aldehyde in the presence of *tert*-butylhydroperoxide (*t*-BuOOH) as an oxidizing agent. It has been shown that at 70 °C with constant reaction conditions, conversion of styrene is maximum in 1, 2-dichloroethane among all other solvents [99]. The catalytic efficiency of ferric hydrogen sulfate supported on silica-coated nickel ferrite (NiFe<sub>2</sub>O<sub>4</sub>@SiO<sub>2</sub>-FHS) was examined by one-pot synthesis of 1, 8-dioxodecahydroacridines by mixing aromatic aldehyde (1 mmol), dimedone (2 mmol), and ammonium acetate or aromatic amine (1 mmol) at 80 °C. The reaction was also carried out in the absence of the catalyst, where no product was obtained. The best result was found using 0.025 g of catalyst at 80 °C under solvent-free conditions [100]. The mixed metal ferrite CoMn<sub>0.2</sub>Fe<sub>1.8</sub>O<sub>4</sub> was used as a catalyst for the reduction reaction of nitroarenes to corresponding aromatic amines. The sol-gel method was employed to fabricate the catalyst, and an average particle diameter was found to be 20 nm. The reaction kinetics was also analyzed using 2-nitroaniline as the model one under UV-Visible spectroscopy, where the reduction reaction followed the pseudo-first-order kinetics [56].

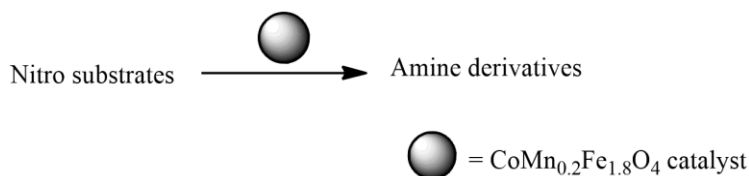


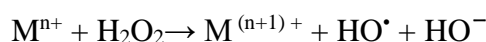
**Figure 6.** Conversion of nitroarenes using CoMn<sub>0.2</sub>Fe<sub>1.8</sub>O<sub>4</sub> nanoparticles.

The electrocatalytic activity of larger-sized spinel NiFe<sub>2</sub>O<sub>4</sub> particles (up to 500  $\mu$ m) for hydrogen evolution reaction (HER) in alkaline water electrolysis provided an active material [101]. The electrocatalytic activity was also tested for nickel ferrites in hydrogen evolution reaction with varying compositions where the trend was found to be Fe<sub>3</sub>O<sub>4</sub>  $\leq$  Ni<sub>0.6</sub>Fe<sub>2.4</sub>O<sub>4</sub>  $\leq$  Ni<sub>0.2</sub>Fe<sub>2.8</sub>O<sub>4</sub>  $\leq$  Ni<sub>0.8</sub>Fe<sub>2.8</sub>O<sub>4</sub>  $\leq$  Ni<sub>0.4</sub>Fe<sub>2.6</sub>O<sub>4</sub> [102]. Pyrazolopyridine derivatives were synthesized by a four-component reaction of hydrazine hydrate, ethyl acetoacetate, aromatic aldehydes, and ammonium acetate in the presence of mesoporous halloysite nanotubes (HNTs) modified by CuFe<sub>2</sub>O<sub>4</sub> nanoparticles (CuFe<sub>2</sub>O<sub>4</sub>@HNTs). Also, the reusability of the catalyst was tested, resulting in no significant decrease in the activity for eight runs under the same reaction condition [103].  $\alpha$ ,  $\beta$ -unsaturated ketones were synthesized using CoFe<sub>2</sub>O<sub>4</sub> nanoparticles (40-50 nm) in ethanol from corresponding aromatic aldehydes, and aryl ketones also provided satisfactory results [23].

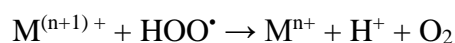
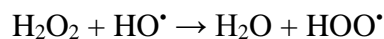
### 3.2. Photocatalytic degradation.

The application of ferrites as photocatalysts is extensively studied mostly for the degradation of dye, a major class of organic contaminants. Hydrogen peroxide (H<sub>2</sub>O<sub>2</sub>) assisted oxidative degradation of dye using ferrite photocatalyst is an effective and well-known experimental area where a Fenton-type reaction between the metal cation and H<sub>2</sub>O<sub>2</sub> takes place, followed by the production of reactive oxygen species from the decomposition of H<sub>2</sub>O<sub>2</sub> [104].

The proposed mechanism says that in this oxidation process, initially, HO<sup>•</sup> is generated from H<sub>2</sub>O<sub>2</sub> decomposition.



This HO<sup>•</sup> radical reacts with H<sub>2</sub>O<sub>2</sub>, and peroxide radical (HOO<sup>•</sup>) is generated, and the reaction between this HOO<sup>•</sup> and M<sup>(n+1)+</sup> produces oxygen (O<sub>2</sub>). HO<sup>•</sup> radicals can also react with the organic species (e.g., dye) in the oxidation process [105].



Here, the photocatalytic activity of spinel ferrites for some commonly studied dyes is reviewed below.

### 3.2.1. Degradation of methylene blue (MB).

MB is one of the most commonly studied dyes used as a redox indicator, staining agent in medical diagnosis, or dyestuff in the textile industry. A cationic dye chemically called methylthioninium chloride can contaminate water when disposed of these effluents untreated. Spinel ferrites proved themselves a potential catalyst for the degradation of MB and other dyes responsible for water pollution [106].

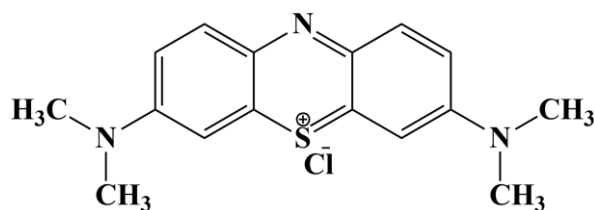


Figure 7. Structure of methylene blue.

Rate of degradation of dye using photocatalyst depends on various parameters like pH, amount and morphology of catalyst, temperature, dye concentration etc. Visible light induced Co<sub>x</sub>Zn<sub>1-x</sub>Fe<sub>2</sub>O<sub>4</sub> (x = 0.0, 0.1, 0.2, 0.3, 0.4 and 0.5) with the aid of 0.1 ml 30 % H<sub>2</sub>O<sub>2</sub> was used to degrade MB dye showed maximum degradation of 77% in 1 hour when x = 0.5. ZnFe<sub>2</sub>O<sub>4</sub> (x = 0.0) showed the least degradation (65%) and the percentage increased with the increase of cobalt content. This is because, when Co<sup>2+</sup> was introduced to ZnFe<sub>2</sub>O<sub>4</sub>, it tended to occupy the octahedral sites having larger volume [107]. Sol-gel synthesis of CoMn<sub>x</sub>Fe<sub>2-x</sub>O<sub>4</sub> (x = 0.2, 0.4, 0.6, 0.8 and 1.0) used to oxidative degradation of MB under visible light as well as in dark showed the degradation increased drastically for CoMn<sub>0.2</sub>Fe<sub>1.8</sub>O<sub>4</sub> in light than dark in presence of 5% H<sub>2</sub>O<sub>2</sub>. Although, for other manganese contents (x = 0.4, 0.6, 0.8 and 1.0) the variation between light and dark is less. Overall, the catalytic activity is increased in the order of CoMnFeO<sub>4</sub> > CoMn<sub>0.8</sub>Fe<sub>1.2</sub>O<sub>4</sub> > CoMn<sub>0.6</sub>Fe<sub>1.4</sub>O<sub>4</sub> > CoMn<sub>0.4</sub>Fe<sub>1.6</sub>O<sub>4</sub> > CoMn<sub>0.2</sub>Fe<sub>1.8</sub>O<sub>4</sub> > CoFe<sub>2</sub>O<sub>4</sub> [104]. Experiments based on copper substituted cobalt-zinc ferrite showed no photocatalytic activity in absence of hydrogen peroxide, but complete degradation was obtained after 90 mins in presence of H<sub>2</sub>O<sub>2</sub> [108]. Both Ni<sub>x</sub>Zn<sub>1-x</sub>Fe<sub>2</sub>O<sub>4</sub> (x = 0.0, 0.2, 0.4, 0.6, 0.8 and 1.0) and Ni<sub>x</sub>Mn<sub>1-x</sub>Fe<sub>2</sub>O<sub>4</sub> (x = 0.0, 0.2, 0.4, 0.6, 0.8 and 1.0) nanoparticles showed efficiency towards the degradation of MB, the activity increased from x = 0.0-0.6 then decreased for x = 0.8-1.0 [109, 110].

**Table 3.** Dye photocatalytic degradation efficiency of spinel ferrites.

Dye	Catalyst	Irradiation Source	Irradiation period	Degradation percentage	Ref.
MB	Co <sub>0.5</sub> Zn <sub>0.5</sub> Fe <sub>2</sub> O <sub>4</sub>	Visible	1 h	77 %	[107]
MB	Titania-silica/ CoFe <sub>2</sub> O <sub>4</sub>	UV	40 min	98.30%	[111]
MB	MgFe <sub>2</sub> O <sub>4</sub>	Visible	50 min	95%	[112]
MB	rGO/ZnFe <sub>2</sub> O <sub>4</sub>	Visible	120 min	99.23%	[113]
MO	CoFe <sub>2</sub> O <sub>4</sub> -Fe <sub>3</sub> O <sub>4</sub>	UV	5 h	93%	[114]
MO	NiFe <sub>2</sub> O <sub>4</sub>	Visible	5 h	71%	[115]
MO	ZnFe <sub>2</sub> O <sub>4</sub> /TiO <sub>2</sub>	Visible	4 h	84%	[116]
MO	CuFe <sub>2</sub> O <sub>4</sub>	UV	90 min	53%	[117]
RhB	Ni <sub>0.8</sub> Zn <sub>0.2</sub> Fe <sub>2</sub> O <sub>4</sub>	Visible	180 min	98.48%	[118]
RhB	SrFe <sub>2</sub> O <sub>4</sub> /g-C <sub>3</sub> N <sub>4</sub>	Visible	40 min	~100%	[119]
RhB	Ag <sub>3</sub> PO <sub>4</sub> @MgFe <sub>2</sub> O <sub>4</sub> <sup>a</sup>	Visible	20 min	98%	[120]
RhB	ZnFe <sub>2</sub> O <sub>4</sub> <sup>b</sup>	Visible	40 min	97.5%	[121]
CR	CdFe <sub>2</sub> O <sub>4</sub>	Microwave	10 min	94.40%	[122]
CR	Co <sub>0.5</sub> Cu <sub>0.5</sub> Fe <sub>2</sub> O <sub>4</sub>	Visible	90 min	~71%	[123]
CR	CoFe <sub>2</sub> O <sub>4</sub>	Visible	90 min	~69%	[123]
CR	MnFe <sub>2</sub> O <sub>4</sub> /TA/ZnO	Visible	90 min	84.20%	[124]

a = 10% concentration; b = Succinic acid-assisted synthesized particles; MB = methylene blue; MO = methyl orange; RhB = rhodamine B; CR = congo red.

### 3.2.2. Degradation of methyl orange (MO)

Methyl orange is a water-soluble azo-dye commonly used as an acid-base indicator. It is a widely used organic dye discharged in water from textile, food, paper, printing, etc.

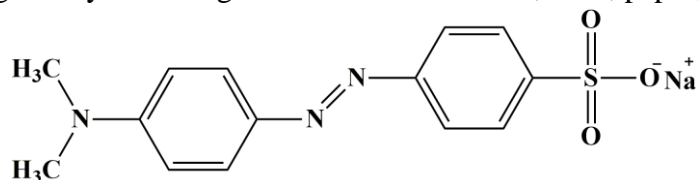


**Figure 8.** Structure of methyl orange

The catalytic activity of NiFe<sub>2</sub>O<sub>4</sub> synthesized by the co-precipitation method was evaluated by the degradation of MO dye under direct sunlight. No significant degradation was observed in the dark, while about 72% degradation was observed within 5 hours of direct sunlight hence concluded this as a suitable heterogeneous photocatalyst [115]. Again, the core-shell NiFe<sub>2</sub>O<sub>4</sub>@TiO<sub>2</sub> was employed as a photocatalyst under ultraviolet light radiation and showed positive results for MO dye degradation. In this case, degradation efficiency increased with the increase of TiO<sub>2</sub> percentage. Degradation efficiency for 10% TiO<sub>2</sub> was 72.69% and for 40% TiO<sub>2</sub> efficiency was 90.06%. The recovered core-shell catalyst was used for ten successive runs without any significant loss of photoactivity [125]. The ultraviolet light radiated photodegradation of MO dye was also carried out using nanocrystalline copper ferrite (CuFe<sub>2</sub>O<sub>4</sub>). Found the degradation efficiency of 53% after 90 mins of UV light irradiation [117]. A more significant result was obtained from MnFe<sub>2</sub>O<sub>4</sub> for oxidative degradation of MO. In the presence of 1 mL, H<sub>2</sub>O<sub>2</sub> 98% degradation of MO dye was observed after 4 hours. This high activity might be obtained from the high specific surface area and active absorbed oxygen species [126].

### 3.2.4. Degradation of rhodamine B (RhB).

RhB is an organic chloride salt that is amphoteric. It contains a xanthene core, thus having a property of fluorescence. It is extensively used in fluorescence microscopy, fluorescence correlation spectroscopy, ELISA, etc. It can cause serious health danger to human beings as well as a threat to the aquatic environment.

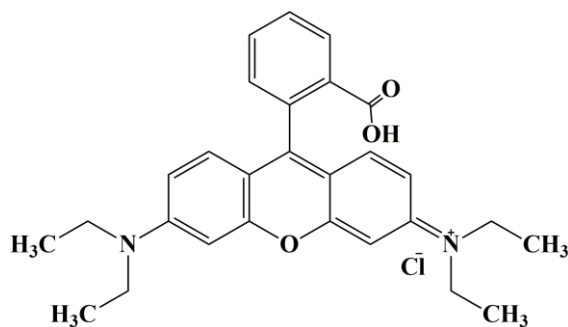


**Figure 9.** Structure of RhB dye.

Succinic acid-assisted hydrothermal synthesis of  $\text{ZnFe}_2\text{O}_4$  with two different morphological properties was studied as a photocatalyst for the degradation of RhB dye. Zinc ferrite synthesized with the aid of succinic acid was labeled as  $\text{ZnFe}_2\text{O}_4\text{-S1}$ , having a regular morphology of cube-shaped particles of 8-18 nm. And particle synthesized using the same procedure except for the addition of any succinic acid was labeled as  $\text{ZnFe}_2\text{O}_4\text{-S2}$ , having an irregular flake-shaped structure with the edge length of 7-13 nm. The degradation efficiency of the photocatalyst S1 was 97.5%, and S2 was 70% after 40 min under visible light. This might result from the high crystallinity and smaller particle size. Also, the photocatalytic activity of the S1 sample was unchanged till the three-cycle experiment [121]. Visible light-induced photocatalytic activity of RhB using zinc doped cobalt ferrite,  $\text{Co}_{1-x}\text{Zn}_x\text{Fe}_2\text{O}_4$  ( $x = 0.0, 0.1, 0.2, 0.3, 0.4$  and  $0.5$ ) and magnesium doped cobalt ferrite,  $\text{Co}_{1-x}\text{Mg}_x\text{Fe}_2\text{O}_4$  ( $x = 0.0, 0.1, 0.2, 0.3, 0.4$  and  $0.5$ ) accomplished almost similar results. The maximum degradation efficiency was 99.5% when  $x = 0.4$  for both the catalysts. Pure  $\text{CoFe}_2\text{O}_4$  showed a minimum efficiency of 73%. And in both cases, degradation efficiency decreased after the maximum, i.e., for  $x = 0.5$ , this might happen due to the structural changes happening due to doping saturation (Co: Zn/Co: Mg = 50:50) [127, 128]. Nickel substituted zinc ferrite,  $\text{Ni}_x\text{Zn}_{1-x}\text{Fe}_2\text{O}_4$  ( $x = 0.0, 0.2, 0.4, 0.6, 0.8,$  and  $1.0$ ) showed a more significant efficiency of 98.48% under visible light after 180 mins. The highest efficiency was observed when  $x = 0.8$ , as it has the highest surface area, thus increasing the number of active sites [119].

### 3.2.5. Degradation of congo red (CR).

Congo red is another commonly used azo dye used as an acid-base indicator. However, its use to dye cotton has been limited but used in histology to stain tissues for microscopic examination. Treatment of this dye effluent is extremely important as it is found to be carcinogenic in nature.

Hydrothermal synthesis of cadmium ferrite,  $\text{CdFe}_2\text{O}_4$  with a narrow size range (20-30 nm) showed excellent efficiency for the degradation of congo red where almost 94.4% of CR dye was degraded within 10 mins under microwave (MW) irradiation. However, the efficiency was only 26.5% unless any MW light radiation thus proved the particle as a prominent photocatalyst [122]. Electrochemical treatment of CR in a microbial fuel cell (MFC) using  $\text{MgFe}_2\text{O}_4$  as an anode modifier also degraded the dye successfully by an electron transport system with electrical energy generation. Where degradation of CR produced aromatic amine, another hazardous material, was also treated to break down to simple compounds [129]. Copper substituted cobalt ferrite,  $\text{Co}_{0.5}\text{Cu}_{0.5}\text{Fe}_2\text{O}_4$  was found to be more effective for the degradation of CR (~71%) than the  $\text{CoFe}_2\text{O}_4$  alone (~69%) under visible light [123]. Magnetically Separable  $\text{MnFe}_2\text{O}_4/\text{TA}/\text{ZnO}$  nanocomposites also degraded the CR dye in the presence of

visible light for 84.2% in 90 min, while  $\text{MnFe}_2\text{O}_4$  or  $\text{ZnO}$  alone couldn't degrade significantly (46.1% and 11.3%, respectively). Moreover, no catalytic activity is observed in the absence of light radiation [124].

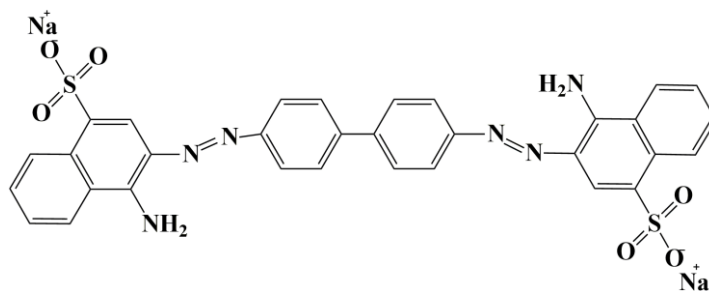


Figure 10. Structure of congo red dye.

#### 4. Conclusions

Structure, morphology, and particle size determine the catalytic properties of spinel ferrites, and the synthetic methods of the particle regulate these. In this review, some commonly pronounced methods to synthesize spinel ferrites have been discussed; different parameters' effect on particle size is also presented. Spinel ferrites possess excellent catalytic properties. They have been corroborated as heterogeneous catalysts in organic synthesis and opened a new pathway to researchers. The catalytic properties in the photo-irradiated oxidation process carried out a fruitful result in the degradation of various organic dyes. However, ferrites, when combined with other particles, i.e., core@ shell structure, the catalytic properties increase significantly.

#### Funding

This research received no external funding.

#### Acknowledgments

This research has no acknowledgments.

#### Conflicts of Interest

The authors declare no conflict of interest.

#### References

1. Ramesh, S.; Dhanalakshmi, B.; Chandra Sekhar, B.; Subba Rao, P. S. V.; Parvatheeswara Rao, B. Structural and magnetic studies on Mn-doped Ni–Zn ferrite nanoparticles. *Appl. Phys. A* **2016**, *122*, 1–8, <https://doi.org/10.1007/s00339-016-0517-6>.
2. Sathiyapriya, A.; Geetha, D.; Kavitha, N. Effect of Al substitution on the structural, electric and impedance behavior of cobalt ferrite. *Vacuum* **2019**, *160*, 453–460, <https://doi.org/10.1016/j.vacuum.2018.12.004>.
3. Khan, S. B.; Irfan, S.; Lee, S. L. Influence of  $\text{Zn}^{+2}$  Doping on Ni-Based Nanoferrites;  $\text{Ni}_{1-x}\text{Zn}_x\text{Fe}_2\text{O}_4$ . *Nanomaterials* **2019**, *9*, 2–17, <https://doi.org/10.3390/nano9071024>.
4. Sathiyamurthy, K.; Rajeevgandhi, C.; Gunganathan, L.; Bharanidharan, S.; Savithiri, S. Enhancement of magnetic, supercapacitor applications and theoretical approach on cobalt-doped zinc ferrite nanocomposites. *J Mater Sci: Mater. Electron.* **2021**, *32*, 11593–11606, <https://doi.org/10.1007/s10854-021-05764-2>.
5. Manikandan, A.; Slimani, Y.; Dinesh, A.; Khan, A.; Thanrasu, K.; Baykal, A.; Jaganathan, S.K.; Dzudzevic-Cancar, H.; Asiri, A. M. Perovskite's potential functionality in a composite structure. *Hybr. Perov. Comp. Mater.* **2021**, 181–202, <https://doi.org/10.1016/B978-0-12-819977-0.00008-1>.
6. Kefeni, K. K.; Msagati, T. A. M.; Mamba, B. B. Ferrite nanoparticles: Synthesis, characterisation and

- applications in electronic device. *Mater. Sci. Eng. B.* **2017**, *215*, 37–55, <https://doi.org/10.1016/j.mseb.2016.11.002>.
7. Khan M. A.; Sabir M.; Mahmood A.; Asghar M.; Mahmood K.; Khan M. A.; Ahmad I.; Sher M.; Warsi M. F. High frequency dielectric response and magnetic studies of  $Zn_{1-x}Tb_xFe_2O_4$  nanocrystalline ferrites synthesized via micro-emulsion technique. *J. Magn. Magn. Mater.* **2014**, *360*, 188–192, <https://doi.org/10.1016/j.jmmm.2014.02.059>.
  8. Gonçalves, M. J.; Rocha, P. D.; Silva, T.N. M.; Martins, R. P.; Nossol, E.; Angnes, L.; Rout, S. C.; Rodrigo, A. A. M. Feasible strategies to promote the sensing performances of spinel  $MCo_2O_4$  (M=Ni, Fe, Mn, Cu and Zn) based electrochemical sensors: A review *J. Mater. Chem. C* **2021**, *9*, 7852-7887, <https://doi.org/10.1039/D1TC01550H>.
  9. Ayyappan, S.; Mahadevan, S.; Chandramohan, P.; Srinivasan, M. P.; Philip, J.; Raj B. Influence of  $Co^{2+}$  Ion concentration on the size, magnetic properties, and purity of  $CoFe_2O_4$  Spinel ferrite nanoparticles. *J. Phys. Chem. C* **2010**, *114*, 6334–6341, <https://doi.org/10.1021/jp911966p>.
  10. Shahjuee, T.; MortezaMasoudpanah, S.; MohammadMirkazemi, S. Coprecipitation Synthesis of  $CoFe_2O_4$  Nanoparticles for Hyperthermia. *J. Ultrafine Grained Nanostructured Mater.* **2017**, *50*, 105–110, <https://doi.org/10.22059/JUFGNSM.2017.02.04>.
  11. Kefeni, K. K.; Mamba, B. B.; Msagati, T. A. M. Application of spinel ferrite nanoparticles in water and wastewater treatment: A review. *Sep. Purif. Technol.* **2017**, *188*, 399–422, <https://doi.org/10.1016/j.seppur.2017.07.015>.
  12. Mayeen A.; Sajan A.K.; Kalarikkal N. Surface Chemistry and Properties of Magnetic Nanoparticles. In: *Magnetic Nanoparticles: A New Platform for Drug Delivery*; 1<sup>st</sup> ed.; Joshy K.S., Sabu T., Thakur V.K., Eds.; Springer, Singapore, 2021; pp. 31-44; ISBN: 978-981-16-1260-2.
  13. Gul, S.; Yousuf, M. A.; Anwar, A.; Warsi, M. F.; Agboola, P. O.; Shakir, I.; Shahid, M. Al-substituted zinc spinel ferrite nanoparticles: Preparation and evaluation of structural, electrical, magnetic and photocatalytic properties. *Ceram. Int.* **2020**, *46*, 14195–14205, <https://doi.org/10.1016/j.ceramint.2020.02.228>.
  14. Kurian, M.; Nair, D. S. On the efficiency of cobalt zinc ferrite nanoparticles for catalytic wet peroxide oxidation of 4-chlorophenol. *J. Environ. Chem. Eng.* **2014**, *2*, 63–69, <https://doi.org/10.1016/j.jece.2013.11.026>.
  15. Sanchez-Lievanos, K. R.; Stair, J. L.; Knowles, K.E. Cation Distribution in Spinel Ferrite Nanocrystals: Characterization, Impact on their Physical Properties, and Opportunities for Synthetic Control. *Inorg. Chem.* **2021**, *60*, 7, 4291–4305, <https://doi.org/10.1021/acs.inorgchem.1c00040>.
  16. Ahmad, I.; Abbas, T.; Islam, M. U.; Maqsood, A. Study of cation distribution for Cu-Co nanoferrites synthesized by the sol-gel method. *Ceram. Int.* **2013**, *39*, 6735–6741, <https://doi.org/10.1016/j.ceramint.2013.02.001>.
  17. Shahane, G. S.; Kumar, A.; Arora, M.; Pant, R. P.; Lal, K. Synthesis and characterization of Ni-Zn ferrite nanoparticles. *J. Magn. Magn. Mater.* **2010**, *322*, 1015–1019, <https://doi.org/10.1016/j.jmmm.2009.12.006>.
  18. Pawar, R. A.; Shirsath, S. E.; Kadam, R. H.; Joshi, R. P.; Patange, S. M. Synthesis and magnetic properties of  $Cu_{0.7}Zn_{0.3}Al_xFe_{2-x}O_4$  nanoferrites using egg-white method. *J. Magn. Magn. Mater.* **2013**, *339*, 138–141, <https://doi.org/10.1016/j.jmmm.2013.03.006>.
  19. Bromho, T. K.; Ibrahim, K.; Kabir, H.; Rahman, M. M.; Hasan, K.; Ferdous, T.; Taha, H.; Altarawneh, M.; Jiang, Z.T. Understanding the impacts of  $Al^{+3}$ -substitutions on the enhancement of magnetic, dielectric and electrical behaviors of ceramic processed nickel-zinc mixed ferrites: FTIR assisted studies. *Mater. Res. Bull.* **2018**, *97*, 444–451, <https://doi.org/10.1016/j.materresbull.2017.09.013>.
  20. Tatarchuk, T.; Bououdina, M.; Judith Vijaya, J.; John Kennedy, L. Spinel ferrite nanoparticles: Synthesis, crystal structure, properties, and perspective applications. *Springer Proc. Phys.* **2017**, *195*, 305–325, [https://doi.org/10.1007/978-3-319-56422-7\\_22](https://doi.org/10.1007/978-3-319-56422-7_22).
  21. Paswan, S.K.; Kumar, P.; Singh, R.K.; Shukla, S.K.; Kumar, L. Spinel Ferrite Magnetic Nanoparticles: An Alternative for Wastewater Treatment. *Pollutants and Water Management: Resources, Strategies and Scarcity* 1<sup>st</sup> ed. John Wiley & Sons Ltd; **2021**, 273-305, <https://doi.org/10.1002/9781119693635.ch11>.
  22. Pardeshi, S. K.; Pawar, R. Y. Optimization of reaction conditions in selective oxidation of styrene over fine crystallite spinel-type  $CaFe_2O_4$  complex oxide catalyst. *Mater. Res. Bull.* **2010**, *45*, 609–615, <https://doi.org/10.1016/j.materresbull.2010.01.011>.
  23. Senapati K. K.; Phukan P. Magnetically separable cobalt ferrite nanocatalyst for aldol condensations of aldehydes and ketones. *Bull. Catal. Soc. Indian.* **2011**, *9*, 1-8.
  24. Lassoued, A.; Lassoued, M. S.; Karolak, F. Synthesis, structural, optical, morphological and magnetic

- characterization of copper substituted nickel ferrite ( $\text{Cu}_x\text{Ni}_{1-x}\text{Fe}_2\text{O}_4$ ) through co-precipitation method. *J. Mater. Sci. Mater. Electron.* **2017**, *28*, 18480-18488, <https://doi.org/10.1007/s10854-017-7795-4>.
25. Maaz, K. S.; Karim, A.; Mashiattullah, J.; Liu, M. D.; Hou, Y. M.; Sun, J. L.; Duan, H. J.; Yao, D.; Y. F. Chen. Structural analysis of nickel doped cobalt ferrite nanoparticles prepared by co-precipitation route. *Phys. B Phys. Condens. Matter.* **2009**, *404*, 3947–3951, <https://doi.org/10.1016/j.physb.2009.07.134>.
  26. Vadivel, M.; Babu, R. R.; Arivanandhan, M.; Ramamurthi, K.; Hayakawa, Y. Role of SDS surfactant concentrations on the structural, morphological, dielectric and magnetic properties of  $\text{CoFe}_2\text{O}_4$  nanoparticles. *RSC Adv.* **2015**, *5*, 27060-27068, <https://doi.org/10.1039/C5RA01162K>.
  27. Rahman, S.; Nadeem, K.; Anis-ur-rehman, M.; Mumtaz, M. Structural and magnetic properties of ZnMg-ferrite nanoparticles prepared using the co-precipitation method. *Ceram. Int.* **2013**, *39*, 5235–5239, <https://doi.org/10.1016/j.ceramint.2012.12.023>.
  28. Zipare, K.; Dhumal, J.; Bandgar, S.; Mathe, V.; Shahane, G. Superparamagnetic Manganese Ferrite Nanoparticles : Synthesis and Magnetic Properties. **2015**, *1*, 178–182.
  29. Dabagh, S.; Chaudhary, K.; Haider, Z.; Ali, J. Study of structural phase transformation and hysteresis behavior of inverse-spinel a-ferrite nanoparticles synthesized by co-precipitation method. *Results Phys.* **2018**, *8*, 93–98, <https://doi.org/10.1016/j.rinp.2017.11.033>.
  30. Pathak, T. K.; Vasoya, N. H.; Natarajan, T. S.; Modi, K. B.; Tayade, R. J. Photocatalytic degradation of aqueous nitrobenzene solution using nanocrystalline Mg-Mn ferrites. **2013**, *764*, 116–129, <https://doi.org/10.4028/www.scientific.net/MSF.764.116>.
  31. Manouchehri, S.; Benehi, S. T. M.; Yousefi, M. H. Effect of Aluminum Doping on the Structural and Magnetic Properties of Mg-Mn Ferrite Nanoparticles Prepared by Coprecipitation Method. *J. Supercond. Nov. Magn.* **2016**, *29*, 2179-2188, <https://doi.org/10.1007/s10948-016-3546-7>.
  32. Vaidyanathan, G. & Sendhilnathan, S. Characterization of  $\text{Co}_{1-x}\text{Zn}_x\text{Fe}_2\text{O}_4$  nanoparticles synthesized by co-precipitation method. *Physica B: Condensed Matter.* **2008**, *403*, 2157–2167, <https://doi.org/10.1016/j.physb.2007.08.219>.
  33. Gul, I. H.; Abbasi, A. Z.; Amin, F.; Anis-ur-Rehman, M.; Maqsood, A. Structural, magnetic and electrical properties of  $\text{Co}_{1-x}\text{Zn}_x\text{Fe}_2\text{O}_4$  synthesized by co-precipitation method. *J. Magn. Magn. Mater.* **2007**, *311*, 494-499, <https://doi.org/10.1016/j.jmmm.2006.08.005>.
  34. Limaye, M. V.; Singh, S. B.; Date, S. K.; Kothari, D.; Reddy, V. R.; Gupta, A.; Sathe, V.; Choudhary, R. J.; Kulkarni, S. K. High coercivity of oleic acid capped  $\text{CoFe}_2\text{O}_4$  nanoparticles at room temperature. *J. Phys. Chem. B* **2009**, *113*, 9070–9076, <https://doi.org/10.1021/jp810975v>.
  35. Yang, L.; Zhang, Y.; Liu, X.; Jiang, X.; Zhang, Z.; Zhang, T.; Zhang, L. The investigation of synergistic and competitive interaction between dye Congo red and methyl blue on magnetic  $\text{MnFe}_2\text{O}_4$ . *Chem. Eng. J.* **2014**, *246*, 88–96, <https://doi.org/10.1016/j.cej.2014.02.044>.
  36. Maaz, K.; Karim, S.; Mumtaz, A.; Hasanain, S. K.; Liu, J.; Duan, J.L. Synthesis and magnetic characterization of nickel ferrite nanoparticles prepared by co-precipitation route. *J. Magn. Magn. Mater.* **2009**, *321*, 1838–1842, <https://doi.org/10.1016/j.jmmm.2008.11.098>.
  37. Shahraki, R. R.; Ebrahimi, M.; Ebrahimi, S. A. S.; Masoudpanah, S. M.; Structural characterization and magnetic properties of superparamagnetic zinc ferrite nanoparticles synthesized by the co-precipitation method. *J. Magn. Magn. Mater.* **2012**, *324*, 3762–3765, <https://doi.org/10.1016/j.jmmm.2012.06.020>.
  38. Vadivel, M.; Babu, R. R.; Sethuraman, K.; Ramamurthi, K.; Arivanandhan, M. Synthesis , structural , dielectric , magnetic and optical properties of Cr substituted  $\text{CoFe}_2\text{O}_4$  nanoparticles by co-precipitation method. *J. Magn. Magn. Mater.* **2014**, *362*, 122–129, <https://doi.org/10.1016/j.jmmm.2014.03.016>.
  39. Victory, M.; Pant, R. P.; Phanjoubam, S. Synthesis and characterization of oleic acid coated Fe–Mn ferrite based ferrofluid. *Mater. Chem. Phys.* **2020**, *240*, 122210, <https://doi.org/10.1016/j.matchemphys.2019.122210>.
  40. Bhandare, S. V.; Kumar, R.; Anupama, A.V.; Choudhary, H.K.; Jali, V.M.; Sahoo, B. Mechanistic insights into the sol-gel synthesis of complex (quaternary) Co–Mn–Zn-spinel ferrites: An annealing dependent study. *Ceram. Int.* **2020**, *46*, 17400-17415, <https://doi.org/10.1016/j.ceramint.2020.04.031>.
  41. Yadav, R.S.; Havlica, J.; Hnatko, M.; Šajgalík, P.; Alexander, C.; Palou, M.; Bartoničková, E.; Boháč, M.; Frajkorová, F.; Masilko, J.; Zmrzlý, M. Magnetic properties of  $\text{Co}_{1-x}\text{Zn}_x\text{Fe}_2\text{O}_4$  spinel ferrite nanoparticles synthesized by starch-assisted sol–gel autocombustion method and its ball milling. *J. Magn. Magn. Mater.* **2015**, *378*, 190-199, <https://doi.org/10.1016/j.jmmm.2014.11.027>.
  42. Yadav, R.S.; Kuřitka, I.; Vilcakova, J.; Urbánek, P.; Machovsky, M.; Masař, M.; Holek, M. Structural, magnetic, optical, dielectric, electrical and modulus spectroscopic characteristics of  $\text{ZnFe}_2\text{O}_4$  spinel ferrite

- nanoparticles synthesized via honey-mediated sol-gel combustion method. *J. Phys. Chem. Solids*. **2017**, *110*, 87-99, <https://doi.org/10.1016/j.jpcs.2017.05.029>.
43. Bobade, D. H.; Rathod, S. M.; Mane, M. L. Sol – gel auto-combustion synthesis , structural and enhanced magnetic properties of Ni<sup>2+</sup> substituted nanocrystalline Mg – Zn spinel ferrite. *Physica B Condens. Matter*. **2012**, *407*, 3700–3704, <https://doi.org/10.1016/j.physb.2012.05.017>.
  44. Jalaiah, K.; Babu, K.V. Structural, magnetic and electrical properties of nickel doped Mn-Zn spinel ferrite synthesized by sol-gel method. *J. Magn. Magn. Mater.* **2017**, *423*, 275-280, <https://doi.org/10.1016/j.jmmm.2016.09.114>.
  45. Shahzadi, K.; Chandio, A.D.; Mustafa, G.; Khalid, M.; Khan, J.K.; Akhtar, M.S.; Gilani, Z.A. Impact of aluminum substitution on the structural and dielectric properties of Ni–Cu spinel ferrite nanoparticles synthesized via sol–gel route. *Opt. Quantum Electron.* **2020**, *52*, 1-17, <https://doi.org/10.1007/s11082-020-02304-w>.
  46. Danks, A.E.; Hall, S.R.; Schnepf, Z. J. M. H. The evolution of ‘sol–gel’ chemistry as a technique for materials synthesis. *Mater. Horiz.* **2016**, *3*, 91-112, <https://doi.org/10.1039/C5MH00260E>.
  47. Raghavender, A. T.; Bili, N.; Skoko, Ž. XRD and IR analysis of nanocrystalline Ni – Zn ferrite synthesized by the sol – gel method. *Mater. Lett.* **2011**, *65*, 677–680, <https://doi.org/10.1016/j.matlet.2010.11.071>.
  48. Elayakumar, K.; Manikandan, A.; Dinesh, A.; Thanrasu, K.; Raja, K.K.; Kumar, R.T.; Slimani, Y.; Jaganathan, S.K.; Baykal, A. Enhanced magnetic property and antibacterial biomedical activity of Ce<sup>3+</sup> doped CuFe<sub>2</sub>O<sub>4</sub> spinel nanoparticles synthesized by sol-gel method. *J. Magn. Magn. Mater.* **2019**, *478*, 140-147, <https://doi.org/10.1016/j.jmmm.2019.01.108>.
  49. Sonia, M. M. L.; Anand, S.; Maria Vinosek, V.; AsisJanifer, M.; Pauline, S.; Manikandan, A. Effect of lattice strain on structure, morphology and magneto-dielectric properties of spinel NiGd<sub>x</sub>Fe<sub>2-x</sub>O<sub>4</sub> ferrite nanocrystallites synthesized by sol-gel route. *J. Magn. Magn. Mater.* **2018**, *466*, 238-251, <https://doi.org/10.1016/j.jmmm.2018.07.017>.
  50. Lobo, L.S.; Kalainathan, S.; Kumar, A.R. Investigation of electrical studies of spinel FeCo<sub>2</sub>O<sub>4</sub> synthesized by sol–gel method. *Superlattices microstruct.* **2015**, *88*, 116-126, <https://doi.org/10.1016/j.spmi.2015.09.010>.
  51. Hakeem, A.; Alshahrani, T.; Muhammad, G.; Alhossainy, M.H.; Laref, A.; Khan, A.R.; Ali, I.; Farid, H.M.T.; Ghrib, T.; Ejaz, S.R.; Khosa, R.Y. Magnetic, dielectric and structural properties of spinel ferrites synthesized by sol-gel method. *J. Mater. Res. Technol.* **2021**, *11*, 158-169, <https://doi.org/10.1016/j.jmrt.2020.12.064>
  52. Bhagwat, V. R.; Humbe, A. V.; More, S. D.; Jadhav, K. M. Sol-gel auto combustion synthesis and characterizations of cobalt ferrite nanoparticles: Different fuels approach. *Mater. Sci. Eng. B* **2019**, *248*, 114388, <https://doi.org/10.1016/j.mseb.2019.114388>.
  53. Javed, M.; Khan, A.A.; Kazmi, J.; Mohamed, M.A.; Khan, M.N.; Hussain, M.; Bilkees, R. Dielectric relaxation and small polaron hopping transport in sol-gel-derived NiCr<sub>2</sub>O<sub>4</sub> spinel chromite. *Mater. Res. Bull.* **2021**, *138*, 111242, <https://doi.org/10.1016/j.materresbull.2021.111242>
  54. Sutka, A.; Mezinskas, G. Sol–gel auto-combustion synthesis of spinel-type ferrite nanomaterials. *Front. Mater. Sci.* **2012**, *6*, 128–141, <https://doi.org/10.1007/s11706-012-0167-3>.
  55. Ashour, A.H.; El-Batal, A.I.; Maksoud, M.A.; El-Sayyad, G.S.; Labib, S.; Abdeltwab, E.; El-Okr, M.M. Antimicrobial activity of metal-substituted cobalt ferrite nanoparticles synthesized by sol–gel technique. *Particuology* **2018**, *40*, 141–151, <https://doi.org/10.1016/j.partic.2017.12.001>.
  56. Goyal, A.; Bansal, S.; Samuel, P.; Kumar, V.; Singhal, S. CoMn<sub>0.2</sub>Fe<sub>1.8</sub>O<sub>4</sub> ferrite nanoparticles engineered by sol–gel technology: an expert and versatile catalyst for the reduction of nitroaromatic compounds. *J. Mater. Chem. A* **2014**, *2*, 18848-18860, <https://doi.org/10.1039/C4TA03900A>.
  57. Habibi, M.H.; Fa, F. Sol – gel combustion synthesis and characterization of nanostructure copper chromite spinel. *J. Therm. Anal. Calorim.* **2013**, *115*, 1329–1333, <https://doi.org/10.1007/s10973-013-3480-x>.
  58. Ibrahim, I.; Ali, I. O.; Salama, T. M.; Bahgat, A. A.; Mohamed, M. M. Synthesis of magnetically recyclable spinel ferrite (MFe<sub>2</sub>O<sub>4</sub>, M= Zn, Co, Mn) nanocrystals engineered by sol gel-hydrothermal technology: High catalytic performances for nitroarenes reduction. *Appl. Catal. B* **2016**, *181*, 389-402, <https://doi.org/10.1016/j.apcatb.2015.08.005>.
  59. Goyal, A.; Bansal, S.; Singhal, S., Facile reduction of nitrophenols: comparative catalytic efficiency of MFe<sub>2</sub>O<sub>4</sub> (M= Ni, Cu, Zn) nano ferrites. *Int. J. Hydrog. Energy*, **2014**, *39*, 4895-4908, <https://doi.org/10.1016/j.ijhydene.2014.01.050>.
  60. Dimesso, L., Pechini processes: an alternate approach of the sol–gel method, preparation, properties, and applications. *Handbook of Sol-Gel Science and Technology*, **2016**, *2*, 1-22, [https://doi.org/10.1007/978-3-319-19454-7\\_123-1](https://doi.org/10.1007/978-3-319-19454-7_123-1).

61. Sivakumar, M.; Kanagesan, S.; Chinnaraj, K.; Babu, R. S.; Nithiyanantham, S. Synthesis, characterization and effects of citric acid and PVA on magnetic properties of  $\text{CoFe}_2\text{O}_4$ . *J. Inorg. Organomet. Polym. Mater.* **2013**, 439–445, <https://doi.org/10.1007/s10904-012-9801-x>.
62. Gupta, N.; Jain, P.; Rana, R.; Shrivastava, S. Current Development in Synthesis and Characterization of Nickel Ferrite Nanoparticle. *Mater. Today Proc.* **2017**, 4, 342–349, <https://doi.org/10.1016/j.matpr.2017.01.031>.
63. Uskoković, V.; Drofenik, M. Synthesis of materials within reverse micelles. *Surf. Rev. Lett.* **2005**, 12, 239–277, <https://doi.org/10.1142/S0218625X05007001>.
64. Lin, X.; Samia, A. C. S. Synthesis, assembly and physical properties of magnetic nanoparticles *J. Magn. Magn. Mater.* **2006**, 305, 100–109, <https://doi.org/10.1016/j.jmmm.2005.11.042>.
65. Mathew, D. S.; Juang, R. An overview of the structure and magnetism of spinel ferrite nanoparticles and their synthesis in microemulsions. *Chem. Eng. Sci.* **2007**, 129, 51–65, <https://doi.org/10.1016/j.ces.2006.11.001>.
66. Pemartin, K.; Solans, C.; Alvarez-quintana, J.; Sanchez-dominguez, M. Synthesis of Mn – Zn ferrite nanoparticles by the oil-in-water microemulsion reaction method. *Colloids Surfaces A Physicochem. Eng. Asp.* **2014**, 451, 161–171, <https://doi.org/10.1016/j.colsurfa.2014.03.036>.
67. Sharifi, I.; Shokrollahi, H.; Mahdi, M.; Safi, R. Magnetic and structural studies on  $\text{CoFe}_2\text{O}_4$  nanoparticles synthesized by co-precipitation, normal micelles and reverse micelles methods. *J. Magn. Magn. Mater.* **2012**, 324, 1854–1861, <https://doi.org/10.1016/j.jmmm.2012.01.015>.
68. Zhou, Z.; Jiang, F.; Lee, T.; Yue, T. Two-step preparation of nano-scaled magnetic chitosan particles using Triton X-100 reversed-phase water-in-oil microemulsion system. *J. Alloys Compd.* **2013**, 581, 843–848, <https://doi.org/10.1016/j.jallcom.2013.07.207>.
69. Foroughi, F.; Hassanzadeh-Tabrizi, S.A.; Amighian, J.; Saffar-Teluri, A. A designed magnetic  $\text{CoFe}_2\text{O}_4$ –hydroxyapatite core–shell nanocomposite for Zn (II) removal with high efficiency. *Ceram. Int.* **2015**, 41, 6844–6850, <https://doi.org/10.1016/j.ceramint.2015.01.133>.
70. Muralidharan, G.; Subramanian, L.; Nallamuthu, S. K.; Santhanam, V.; Kumar, S. Effect of Reagent Addition Rate and Temperature on Synthesis of Gold Nanoparticles in Microemulsion Route. *Ind. Eng. Chem. Res.* **2011**, 50, 8786–8791, <https://doi.org/10.1021/ie2002507>.
71. Murtaza, G.; Ahmad, R.; Hussain, T.; Ayub, R.; Ali, I.; Khan, M.A.; Akhtar, M.N. Structural and magnetic properties of Nd–Mn substituted Y-type hexaferrites synthesized by microemulsion method. *J. Alloys Compd.* **2014**, 602, 122–129, <https://doi.org/10.1016/j.jallcom.2014.02.156>.
72. Abbas, M. K.; Khan, M. A.; Mushtaq, F.; Warsi, M. F.; Sher, M.; Shakir, I.; Aboud, M. F. A. Impact of Dy on structural, dielectric and magnetic properties of Li-Tb-nanoferrites synthesized by micro-emulsion method. *Ceram. Int.* **2017**, 43, 5524–5533, <https://doi.org/10.1016/j.ceramint.2017.01.075>.
73. Yadav, A.; Varshney, D. Structural and Dielectric Properties of Copper-Substituted Mg – Zn Spinel Ferrites. *J. Supercond. Nov. Magn.* **2017**, 30, 1297–1302, <https://doi.org/10.1007/s10948-016-3931-2>.
74. Palacio Gómez, C.A.; BarreroMeneses, C.A.; Matute, A. Structural parameters and cation distributions in solid state synthesized Ni-Zn ferrites. *Materials Science and Engineering: B* **2018**, 236–237, 48–55, <https://doi.org/10.1016/j.mseb.2018.12.003>.
75. Mounkachi, O.; Hamedoun, M.; Belaiche, M.; Benyoussef, A.; Masrour, R.; El Moussaoui, H.; Sajieddine, M. Synthesis and magnetic properties of ferrites spinels  $\text{Mg}_x\text{Cu}_{1-x}\text{Fe}_2\text{O}_4$ . *Phys. B Phys. Condens. Matter* **2012**, 407, 27–32, <https://doi.org/10.1016/j.physb.2011.09.023>.
76. Pandit, R.; Sharma, K. K.; Kaur, P.; Kumar, R. Cation distribution controlled dielectric, electrical and magnetic behavior of  $\text{In}^{3+}$  substituted cobalt ferrites synthesized via solid-state reaction technique. *Mater. Chem. Phys.* **2014**, 148, 988–999, <https://doi.org/10.1016/j.matchemphys.2014.09.009>.
77. Palacio Gómez, C.A.; BarreroMeneses, C.A.; Jaén, J.A. Raman, infrared and Mössbauer spectroscopic studies of solid-state synthesized Ni-Zn ferrites. *J. Magn. Magn. Mater.* **2020**, 505, 166710, <https://doi.org/10.1016/j.jmmm.2020.166710>.
78. Xu, J.; Yang, H.; Fu, W.; Du, K.; Sui, Y.; Chen, J.; Zeng, Y.; Li, M.; Zou, G. Preparation and magnetic properties of magnetite nanoparticles by sol–gel method. *J. Magn. Magn. Mater.* **2007**, 309, 307–311, <https://doi.org/10.1016/j.jmmm.2006.07.037>.
79. De Sousa, M.E.; Fernandez van Raap, M.B.; Rivas, P.C.; Mendoza Zelis, P.; Girardin, P.; Pasquevich, G.A.; Alessandrini, J.L.; Muraca, D.; Sánchez, F.H., Stability and relaxation mechanisms of citric acid coated magnetite nanoparticles for magnetic hyperthermia. *J. Phys. Chem. C* **2013**, 117, 5436–5445, <https://doi.org/10.1021/jp311556b>.
80. Ch, K.; Dhar, S. S. Rapid catalytic degradation of malachite green by  $\text{MgFe}_2\text{O}_4$  nanoparticles in presence of

- H<sub>2</sub>O<sub>2</sub>. *J. Alloys Compd.* **2020**, *828*, 154462, <https://doi.org/10.1016/j.jallcom.2020.154462>.
81. Gangaswamy, D. R. S.; Varma, M. C.; Bharadwaj, S.; Rao, K. S.; Rao, K. H. Comparison Study of Structural and Magnetic Properties of Magnesium-Substituted Nickel – Zinc Ferrites Synthesized by Solid-State and Sol – Gel Routes. *J. Supercond. Nov. Magn.* **2015**, *28*, 3599–3606, <https://doi.org/10.1007/s10948-015-3188-1>.
  82. Chandradass, J.; Kim, K. H. Solvent effects in the synthesis of MgFe<sub>2</sub>O<sub>4</sub>nanopowders by reverse micelle processing. *J. Alloys Compd.* **2011**, *509*, L59–L62, <https://doi.org/10.1016/j.jallcom.2010.10.090>.
  83. Thakur, S.; Katyal, S. C.; Gupta, A.; Reddy, V. R.; Sharma, S. K.; Knobel, M.; Singh, M. Nickel-Zinc Ferrite from Reverse Micelle Process: Structural and Magnetic Properties, Mössbauer Spectroscopy Characterization. *J. Phys. Chem. C* **2009**, *113*, 20785–20794, <https://doi.org/10.1021/jp9050287>.
  84. Nejati, K.; Zabihi, R. Preparation and magnetic properties of nano size nickel ferrite particles using hydrothermal method. *Chem. Central J.* **2012**, *6*, <https://doi.org/10.1186/1752-153x-6-23>.
  85. Allaedini, G.; Masrinda, S.; Payam, T. Magnetic properties of cobalt ferrite synthesized by hydrothermal method. *Int. Nano Lett.* **2012**, *5*, 183–186, <https://doi.org/10.1007/s40089-015-0153-8>.
  86. Singh, G.; Chandra, S. Electrochemical performance of MnFe<sub>2</sub>O<sub>4</sub> nano- ferrites synthesized using thermal decomposition method. *Int. J. Hydrogen Energy* **2017**, *43*, 4058-4066, <https://doi.org/10.1016/j.ijhydene.2017.08.181>.
  87. Gyergyek, S.; Makovec, D.; Kodre, A.; Arčon, I.; Jagodič, M.; Drogenik, M. Influence of synthesis method on structural and magnetic properties of cobalt ferrite nanoparticles. *J. Nano. Research* **2010**, *12*, 1263–1273, <https://doi.org/10.1007/s11051-009-9833-5>.
  88. Das, S.; Manoharan, C.; Venkateshwarlu, M.; Dhamodharan, P. Structural, optical, morphological and magnetic properties of nickel doped cobalt ferrite nanoparticles synthesized by hydrothermal method. *J. Mater. Sci. Mater. Electron.* **2019**, <https://doi.org/10.1007/s10854-019-02355-0>.
  89. Rahmayeni, R.; Oktavia, Y.; Stiadi, Y.; Arief, S. Spinel ferrite of MnFe<sub>2</sub>O<sub>4</sub> synthesized in *Piper betle* Linn extract media and its application as photocatalysts and antibacterial. *J. Dispers. Sci. Technol.* **2020**, 1–10, <https://doi.org/10.1080/01932691.2020.1721011>.
  90. Asiri, S.; Sertkol, M.; Guner, S.; Gungunes, H.; Batoov, K. M.; Saleh, T. A.; Baykal, A. Hydrothermal synthesis of Co<sub>y</sub>Zn<sub>y</sub>Mn<sub>1-2y</sub>Fe<sub>2</sub>O<sub>4</sub>nanoferrites: Magneto-optical investigation. *Ceram. Int.* **2018**, *44*, 5751–5759, <https://doi.org/10.1016/j.ceramint.2017.12.233>.
  91. Li, M.; Liu, X.; Xu, T.; Nie, Y.; Li, H.; Zhang, C. Synthesis and characterization of nanosized MnZn ferrites via a modified hydrothermal method. *J. Magn. Magn. Mater.* **2017**, *439*, 228-235, <https://doi.org/10.1016/j.jmmm.2017.04.015>.
  92. Monfared, A. H.; Zamanian, A.; Beygzadeh, M.; Sharifi, I.; Mozafari, M. A rapid and efficient thermal decomposition approach for the synthesis of manganese-zinc/oleylamine core/shell ferrite nanoparticles. *J. Alloys Compd.* **2016**, *694*, 1090-1095, <https://doi.org/10.1016/j.jallcom.2016.09.253>.
  93. Sharifi, I.; Zamanian, A.; Behnamghader, A. Synthesis and characterization of Fe<sub>0.6</sub>Zn<sub>0.4</sub>Fe<sub>2</sub>O<sub>4</sub> ferrite magnetic nanoclusters using simple thermal decomposition method. *J. Mag. Mag. Mater.* **2016**, *412*, 107–113, <https://doi.org/10.1016/j.jmmm.2016.03.091>.
  94. Herrera, A.P.; Polo-Corrales, L.; Chavez, E.; Cabarcas-Bolivar, J.; Uwakweh, O.N.; Rinaldi, C. Influence of aging time of oleate precursor on the magnetic relaxation of cobalt ferrite nanoparticles synthesized by the thermal decomposition method. *J. Magn. Magn. Mater.* **2013**, *328*, 41–52, <https://doi.org/10.1016/j.jmmm.2012.09.069>.
  95. Sánchez, J.; Cortés-Hernández, D.A.; Escobedo-Bocardo, J.C.; Almanza-Robles, J.M.; Reyes-Rodríguez, P.Y.; Jasso-Terán, R.A.; Bartolo-Pérez, P.; De-León-Prado, L.E. Synthesis of Mn<sub>x</sub>Ga<sub>1-x</sub>Fe<sub>2</sub>O<sub>4</sub> magnetic nanoparticles by thermal decomposition method for medical diagnosis applications. *J. Magn. Magn. Mater.* **2017**, *427*, 227-275, <https://doi.org/10.1016/j.jmmm.2016.10.098>.
  96. Shahjuee, T.; Masoudpanah, S. M.; Mirkazemi, S. M. Thermal Decomposition Synthesis of MgFe<sub>2</sub>O<sub>4</sub> Nanoparticles for Magnetic Hyperthermia. *J. Supercon. Novel Mag.* **2018**, <https://doi.org/10.1007/s10948-018-4834-1>.
  97. Abd, M.; Aleem, E.; Ali, A.; Abu-dief, A. M. CuFe<sub>2</sub>O<sub>4</sub> nanoparticles: An efficient heterogeneous magnetically separable catalyst for Synthesis of some novel propynyl-1H- imidazoles derivatives. *Tetrahedron* **2015**, *71*, 2579-2584, <https://doi.org/10.1016/j.tet.2015.02.057>.
  98. Murthy Y. L. N.; Diwakar, B. S.; Govindh, B.; Nagalakshmi, K.; Viswanath, I. V. K.; Singh, R. Nano copper ferrite : A reusable catalyst for the synthesis of β , γ -unsaturated ketones. *J. Chem. Sci.* **2012**, *124*, 639–645, <https://doi.org/10.1007/s12039-012-0258-9>.

99. Kooti, M.; Afshari, M. Magnetic cobalt ferrite nanoparticles as an efficient catalyst for oxidation of alkenes. *Sci. Iran.* **2012**, *19*, 1991–1995, <https://doi.org/10.1016/j.scient.2012.05.005>.
100. Khojastehnezhad, A.; Rahimizadeh, M.; Eshghi, H.; Moeinpour, F. Ferric hydrogen sulfate supported on silica-coated nickel ferrite nanoparticles as new and green magnetically separable catalyst for. *Chinese J. Catal.* **2014**, *35*, 376–382, [https://doi.org/10.1016/S1872-2067\(14\)60001-2](https://doi.org/10.1016/S1872-2067(14)60001-2).
101. Chanda, D.; Hnát, J. Paidar, M.; Schauer, J.; Bouzek, K. Synthesis and characterization of NiFe<sub>2</sub>O<sub>4</sub> electrocatalyst for the hydrogen evolution reaction in alkaline water electrolysis using different polymer binders. *J. Power Sources* **2015**, *285*, 217–226, <https://doi.org/10.1016/j.jpowsour.2015.03.067>.
102. Abbaspour, A.; Mirahmadi, E. Electrocatalytic hydrogen evolution reaction on carbon paste electrode modified with Ni ferrite nanoparticles. *Fuel* **2013**, *104*, 575–582, <https://doi.org/10.1016/j.fuel.2012.07.016>.
103. Maleki, A.; Hajizadeh, Z.; Salehi, P. Mesoporous halloysite nanotubes modified by CuFe<sub>2</sub>O<sub>4</sub> spinel ferrite nanoparticles and study of its application as a novel and efficient heterogeneous catalyst in the synthesis of pyrazolopyridine derivatives. *Sci. Reports* **2019**, *9*, 5552, <https://doi.org/10.1038/s41598-019-42126-9>.
104. Jauhar, S.; Singhal, S.; Dhiman, M. General Manganese substituted cobalt ferrites as efficient catalysts for H<sub>2</sub>O<sub>2</sub> assisted degradation of cationic and anionic dyes : Their synthesis and characterization. *Applied Catal. A, Gen.* **2014**, *486*, 210–218, <https://doi.org/10.1016/j.apcata.2014.08.020>.
105. Albuquerque, A. S.; Tolentino, M. V. C.; Mendonc, R. De; Macedo, W. A. A. Nanostructured ferrites : Structural analysis and catalytic activity. *Ceramic Int.* **2012**, *38*, 2225–2231, <https://doi.org/10.1016/j.ceramint.2011.10.071>.
106. Hammouche, J.; Gaidi, M.; Columbus, S.; Omari, M.; Enhanced Photocatalytic Performance of Zinc Ferrite Nanocomposites for Degrading Methylene Blue: Effect of Nickel Doping Concentration. *J. Inorg. Organomet. Polym.* **2021**, 1–9, <https://doi.org/10.1007/s10904-021-01960-z>
107. Chahar, D.; Taneja, S.; Bisht, S.; Kesarwani, S.; Thakur, P.; Thakur, A.; Sharma, P.B. Photocatalytic activity of cobalt substituted zinc ferrite for the degradation of methylene blue dye under visible light irradiation. *J. Alloys Compd.* **2021**, *851*, 156878, <https://doi.org/10.1016/j.jallcom.2020.156878>.
108. Bhukal, S.; Singhal, S. Magnetically separable copper substituted cobalt – zinc nano-ferrite photocatalyst with enhanced photocatalytic activity. *Mater. Sci. Semicond. Process.* **2014**, *26*, 467–476, <https://doi.org/10.1016/j.mssp.2014.05.023>.
109. Padmapriya, G.; Manikandan, A.; Krishnasamy, V.; Kumar, S.; Antony, S. A. Spinel Ni<sub>x</sub>Zn<sub>1-x</sub>Fe<sub>2</sub>O<sub>4</sub> (0.0 ≤ x ≤ 1.0) nano-photocatalysts: Synthesis, characterization and photocatalytic degradation of methylene blue dye. *J. Mol. Structure* **2016**, *1119*, 39–47, <https://doi.org/10.1016/j.molstruc.2016.04.049>.
110. Mathubala, G.; Manikandan, A.; Antony, S. A.; Ramar, P. Photocatalytic degradation of methylene blue dye and magneto- optical studies of magnetically recyclable spinel Ni<sub>x</sub>Mn<sub>1-x</sub>Fe<sub>2</sub>O<sub>4</sub> (x = 0.0–1.0) nanoparticles. *J. Mol. Structure* **2016**, *1113*, 79–87, <https://doi.org/10.1016/j.molstruc.2016.02.032>.
111. Harraz, F. A.; Mohamed, R. M.; Rashad, M. M.; Wang, Y. C.; Sigmund, W. Magnetic nanocomposite based on titania – silica/ cobalt ferrite for photocatalytic degradation of methylene blue dye. *Ceram. Int.* **2013**, *40*, 375–384, <https://doi.org/10.1016/j.ceramint.2013.06.012>.
112. Shahid, M.; Jingling, L.; Ali, Z.; Shakir, I.; Warsi, M.F.; Parveen, R.; Nadeem, M Photocatalytic degradation of methylene blue on magnetically separable MgFe<sub>2</sub>O<sub>4</sub> under visible light irradiation. *Mater. Chem. Phys.* **2013**, *139*, 566–571, <https://doi.org/10.1016/j.matchemphys.2013.01.058>.
113. Rani, G. J.; Rajan, M. J. Reduced graphene oxide/ZnFe<sub>2</sub>O<sub>4</sub> nanocomposite as an efficient catalyst for the photocatalytic degradation of methylene blue dye. *Res. Chem. Intermed.* **2016**, *43*, 2669–2690, <https://doi.org/10.1007/s11164-016-2788-0>.
114. Mishra, D.; Senapati, K. K.; Borgohain, C.; Perumal, A. CoFe<sub>2</sub>O<sub>4</sub>–Fe<sub>3</sub>O<sub>4</sub> Magnetic Nanocomposites as Photocatalyst for the Degradation of Methyl Orange Dye. *J. Nanotech.* **2012**, *2012*, 1–6, <https://doi.org/10.1155/2012/323145>.
115. Hirtha; Sendhilnathan, S.; Rajan, P. I.; Adinaveen, T. Synthesis and Characterization of NiFe<sub>2</sub>O<sub>4</sub> Nanoparticles for the Enhancement of Direct Sunlight Photocatalytic Degradation of Methyl Orange. *J. Supercon. Novel Mag.* **2018**, *31*, 3315–3322, <https://doi.org/10.1007/s10948-018-4601-3>.
116. Cheng, P.; Deng, C.; Gu, M.; Shangguan, W. Visible-light responsive zinc ferrite doped titania photocatalyst for methyl orange degradation. *J. Mater. Sci.* **2007**, *42*, 9239–9244, <https://doi.org/10.1007/s10853-007-1902-5>.
117. Vosoughifar, M. Preparation and application of copper ferrite nanoparticles for degradation of methyl orange. *J. Mater. Sci. Mater. Electron* **2016**, *27*, 10449–10453, <https://doi.org/10.1007/s10854-016-5133-x>.
118. Jadhav, S. A.; Somvanshi, S. B.; Khedkar, M. V.; Patade, S. R. Magneto-structural and photocatalytic

- behavior of mixed Ni–Zn nano-spinel ferrites : visible light-enabled active photodegradation of rhodamine B. *Mater. Sci. Mater. Electron.* **2020**, *31*, 11352-11365, <https://doi.org/10.1007/s10854-020-03684-1>.
- 119.Bo, L.; Hu, Y.; Zhang, Z.; Tong, J. Efficient photocatalytic degradation of Rhodamine B catalyzed by SrFe<sub>2</sub>O<sub>4</sub>/g-C<sub>3</sub>N<sub>4</sub> composite under visible light. *Polyhedron* **2019**, *168*, 94–100, <https://doi.org/10.1016/j.poly.2019.04.036>.
- 120.Zhou, T.; Zhang, G.; Ma, P.; Qiu, X.; Zhang, H.; Yang, H.; Liu, G. Efficient degradation of rhodamine B with magnetically separable Ag<sub>3</sub>PO<sub>4</sub>@MgFe<sub>2</sub>O<sub>4</sub> composites under visible irradiation. *Alloys Compd.* **2018**, *735*, 1277-1290, <https://doi.org/10.1016/j.jallcom.2017.11.245>.
- 121.Han, L.; Zhou, X.; Wan, L.; Deng, Y.; Zhan, S. Synthesis of ZnFe<sub>2</sub>O<sub>4</sub> nanoplates by succinic acid-assisted hydrothermal route and their photocatalytic degradation of rhodamine B under visible light. *J. Environmental Chem. Eng.* **2014**, *2*, 123–130, <https://doi.org/10.1016/j.jece.2013.11.031>.
- 122.Shi, W.; Liu, X.; Zhang, T.; Wang, Q.; Zhang, L. Magnetic nano-sized cadmium ferrite as an efficient catalyst for the degradation of Congo red. *RSC Adv.* **2015**, *5*, 51027–51034, <https://doi.org/10.1039/C5RA07591B>.
- 123.Kirankumar, V. S.; Hardik, B; Sumathi, S. Photocatalytic degradation of congo red using copper substituted cobalt ferrite. *Mater. Sci. Eng.* **2017**, *263*, 022027, <https://doi.org/10.1088/1757-899X/263/2/022027>.
- 124.Boutra, B.; Güy, N.; Özacar, M.; Trari, M. Magnetically Separable MnFe<sub>2</sub>O<sub>4</sub>/TA/ZnO Nanocomposites for Photocatalytic Degradation of Congo Red Under Visible Light. *J. Magn. Magn. Mater.* **2019**, *497*, 165994, <https://doi.org/10.1016/j.jmmm.2019.165994>.
- 125.Baig, M. M.; Pervaiz, E.; Afzal, M. J. Catalytic Activity and Kinetic Studies of Core@Shell Nanostructure NiFe<sub>2</sub>O<sub>4</sub>@TiO<sub>2</sub> for Photocatalytic Degradation of Methyl Orange Dye. **2020**, *42*, 531–541.
- 126.Zhang, L.; Wu, Y. Sol-Gel Synthesized Magnetic MnFe<sub>2</sub>O<sub>4</sub> Spinel Ferrite Nanoparticles as Novel Catalyst for Oxidative Degradation of Methyl Orange. *J. Nanomater.* **2013**, *2013*, 1-6, <http://dx.doi.org/10.1155/2013/640940>.
- 127.Sundararajan, M.; Sailaja, V.; Kennedy, L. J.; Vijaya, J. Photocatalytic degradation of rhodamine B under visible light using nanostructured zinc doped cobalt ferrite: kinetics and mechanism. *Ceram. Int.* **2016**, *43*, 540-548, <https://doi.org/10.1016/j.ceramint.2016.09.191>.
- 128.Sundararajan, M.; Kennedy, L. J.; Nithya, P.; Vijaya, J.; Bououdina, M. Visible light driven photocatalytic degradation of rhodamine B using Mg doped cobalt ferrite spinel nanoparticles synthesized by microwave combustion method. *J. Phys. Chem. Solids* **2017**, *108*, 61-75, <https://doi.org/10.1016/j.jpcs.2017.04.002>.
- 129.Khan, N.; Anwer, A. H.; Khan, M. D.; Azam, A., Ibadon, A.; Khan, M. Z. Magnesium Ferrite Spinel as Anode Modifier for the treatment of Congo red and Energy recovery in a Single Chambered Microbial Fuel Cell. *J. Hazard. Mater.* **2021**, *410*, 124561, <https://doi.org/10.1016/j.jhazmat.2020.124561>.